Applied Catalysis A, General 710 (2026) 120682

Contents lists available at ScienceDirect

Applied Catalysis A, General

journal homepage: www.elsevier.com/locate/apcata

Doped In_2O_3/ZrO_2 catalysts to drive selectivity toward DME in one-pot CO_2 hydrogenation

Simona Renda, Jaime Soler, Miguel Menéndez, Javier Herguido *

Catalysis and Reactor Engineering Group (CREG), Aragon Institute of Engineering Research (I3A), Universidad de Zaragoza, Zaragoza 50018, Spain

ARTICLE INFO

Keywords:
Dimethyl ether synthesis
Doped (Cu, Ni, Pd, Pt) In_2O_3/ZrO_2 catalyst
Selectivity modification
4A zeolite
CO_2 hydrogenation

ABSTRACT

This study investigates single-pass dimethyl ether synthesis at mild pressure conditions using novel bifunctional catalysts based on indium-modified formulations and incorporating Ni, Cu, Pt, and Pd as active metals. Additionally, the substitution of the conventional HZSM-5 zeolite with 4A zeolite as the dehydration component was evaluated. Although 4A zeolite exhibited lower dehydration activity, it contributed to an overall improvement in DME selectivity. The incorporation of secondary metals into the In_2O_3-ZrO_2 formulation reduced catalytic activity but enhanced selectivity, ultimately increasing DME yield. The formation of by-products such as light olefins and methane was significantly dependent on the metal used: Ni, Pt, and Pd reduced olefin production, though Ni promoted excessive methane formation across the whole temperature range. Notably, the Pt-based catalyst completely suppressed by-product formation across the temperature range studied. While the In_2O_3-ZrO_2-based catalysts generally displayed lower space–time yields than the commercial reference, they achieved comparable performance at 280 °C. Due to their superior selectivity, these formulations are promising for developing even better performing catalysts, to be excellent candidates in industrial processes, where the operation with recycle loops requires a high product purity.

1. Introduction

Dimethyl ether (DME) used to be a byproduct of methanol synthesis. Nevertheless, due to its versatility as a fuel and as a chemical, the demand for this product rose in the years, leading to dedicated DME synthesis plants [1]. It can serve as precursor for light olefins synthesis or as intermediate in the production of dimethyl sulfate, acetic acid and other organic compounds. However, it has an even greater interest as a fuel, since it can replace liquefied petroleum gas (LPG) for domestic purposes [2] and because it represents an alternative to the widespread diesel fuel. Indeed, its high cetane number (>55) allows to employ DME in conventional engines with minor modifications [3], and its combustion implies minimal particulate matter emissions and the absence of NO_x [4,5]. DME is conventionally synthesized *via* methanol dehydration, but it can be produced in a single step from syngas with the use of the so-called bifunctional catalysts, i.e. formulations that contains both methanol synthesis and dehydration active sites [6,7].

Direct DME synthesis can also be performed through CO_2 hydrogenation. Of course, due to the present environmental concerns, a technology that allows the exploitation of carbon dioxide on one hand, and the utilization of green H_2 from renewable sources on the other hand, is highly captivating [8,9]. Of course, this path presents its drawbacks. The DME direct synthesis from CO_2 has lower yield at thermodynamic equilibrium than its production from CO [10], thus hindering even more the productivity of a process which already has non-negligible restrictions [11]. Direct DME synthesis occurs following Eq.1, which takes place as a reaction in series of Eq.2 and Eq.3.

$$2CO_2 + 6H_2 \rightleftarrows CH_3OCH_3 + 3H_2O \quad \Delta H^0_{298K} = -122.4\ kJ.mol^{-1} \tag{1}$$

$$CO_2 + 3H_2 \rightleftarrows CH_3OH + H_2O \quad \Delta H^0_{298K} = -49.5\ kJ.mol^{-1} \tag{2}$$

$$2CH_3OH \rightleftarrows CH_3OCH_3 + H_2O \quad \Delta H^0_{298K} = -23.4\ kJ.mol^{-1} \tag{3}$$

The reaction is exothermic and accompanied by a decrease in moles, thus DME production is promoted by low temperatures and high pressures, according to the thermodynamic equilibrium. Although the low temperatures are not an issue from an industrial point of view – in fact this would represent a reduction in the cost of the process –, it is a remarkable issue for the kinetic of the reaction. Hence, a balance must be found in having a catalyst with a very low-temperature activation

* Corresponding author.
E-mail address: jhergui@unizar.es (J. Herguido).

https://doi.org/10.1016/j.apcata.2025.120682
Received 14 May 2025; Received in revised form 3 November 2025; Accepted 7 November 2025
Available online 8 November 2025

Table 1
Physical properties and composition of the catalysts.

	SSA (m^2 g^{-1})	V_{micro} (cm^3 g^{-1})	V_{meso} (cm^3 g^{-1})	XRF composition (wt%)		Si/Al ratio
				In_2O_3	Me	
ZrO_2	102	0.067	0.226			
InZr	133	0.085	0.277	10.51 ± 0.13		
Ni/InZr	103	0.063	0.298	9.98 ± 0.12	3.04 ± 0.11	
Cu/InZr	99	0.061	0.199	10.02 ± 0.13	3.12 ± 0.10	
Pd/InZr	121	0.071	0.299	10.21 ± 0.13	0.65 ± 0.04	
Pt/InZr	122	0.072	0.303	10.28 ± 0.13	0.58 ± 0.03	
HZSM−5 (pristine)	367	0.167	0.093			16.6
HZSM−5	267	0.134	0.286			18.7
4A	553	0.226	0.114			1.5

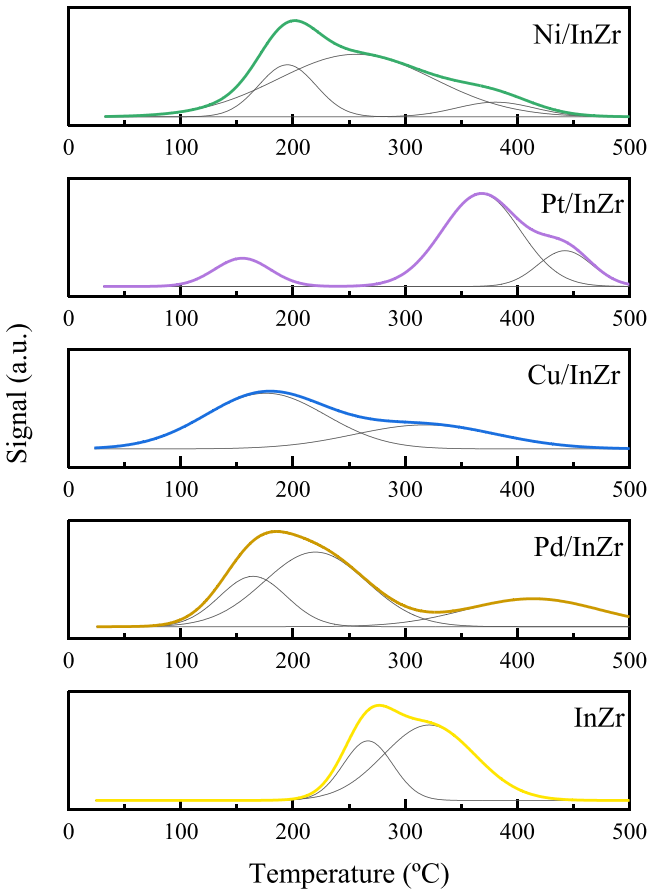

Fig. 1. Reduction profiles for the methanol synthesis catalysts.

threshold or a highly selective catalyst, to avoid competitive reactions when working at higher temperatures.

It is also worth mentioning that, since the overall process is constituted by an in-series reaction, two formulations need to be optimized, the methanol-synthesis catalyst and the dehydration catalyst. Conventionally, copper-zinc based formulations such as CuO-ZnO-Al_2O_3 and CuO-ZnO-ZrO_2 (usually addressed as CZA and CZZ) represent the methanol-synthesis catalyst [12,13], while the dehydration occurs on zeolites or, less often, on alumina. The most employed zeolite to this aim is HZSM-5 [14]. Copper-zinc based catalyst demonstrated high CO_2 conversion, but they do not have a remarkable selectivity toward the desired product. In fact, a significant contribution to CO_2 conversion is given by the reverse water-gas shift reaction (rWGS) according to Eq.4.

$$CO_2 + H_2 \rightleftarrows CO + H_2O \quad \Delta H^0_{298K} = +45\ kJ.mol^{-1} \tag{4}$$

Other side reactions can occur during this process, leading to the synthesis of methane and short-chain paraffins/olefins. To properly account for their production, the general stoichiometry according to Eqs. 5–9 can be considered.

$$CO_2 + 4H_2 \rightleftarrows CH_4 + 2H_2O \quad \Delta H^0_{298K} = -165\ kJ.mol^{-1} \tag{5}$$

$$2CO_2 + 6H_2 \rightleftarrows C_2H_4 + 4H_2O \quad \Delta H^0_{298K} = -128\ kJ.mol^{-1} \tag{6}$$

$$2CO_2 + 7H_2 \rightleftarrows C_2H_6 + 4H_2O \quad \Delta H^0_{298K} = -265\ kJ.mol^{-1} \tag{7}$$

$$3CO_2 + 9H_2 \rightleftarrows C_3H_6 + 6H_2O \quad \Delta H^0_{298K} = -250\ kJ.mol^{-1} \tag{8}$$

$$3CO_2 + 10H_2 \rightleftarrows C_3H_8 + 6H_2O \quad \Delta H^0_{298K} = -374\ kJ.mol^{-1} \tag{9}$$

Recently, it has been reported that In_2O_3/ZrO_2 catalysts can be a promising alternative to the conventional copper-zinc ones for the CO_2-to-methanol synthesis, since they are able to inhibit the CO production. Moreover, some authors observed that indium formulations are less prone to sintering in water-rich environments compared to CZA and CZZ ones. Copper migration and coalescence and Al_2O_3 sintering due to the presence of water are in fact one of the most relevant issues for what concerns the stability of methanol catalysts [15].

Due to the novelty of the formulation, to the best of our knowledge few studies report the employment of indium-based catalysts, compared to the large variety of studies involving conventional CZA and CZZ formulations. In addition, most of the studies on In-based materials have been conducted for the CO/CO_2-to-olefin process, or methanol to olefins (MTO); therefore, DME synthesis is discussed but rarely constitutes the focus of the study. Ateka et al. [16] studied the performances of a In_2O_3/Zr_2O_3/SAPO-34 catalyst, discussing the operating conditions which favored the yield to olefins. Similar considerations have been made by Zhang et al. [17] who evaluate the effect of SAPO-34 structure on the selectivity. The combination of InZr mixed oxide with SAPO-34 for olefine productions was also observed by Su et al. [18], who evaluated the effect on In:Zr ratio. Porta et al. performed an interesting study on the spatial arrangements that could maximize olefins productions [19]. Pechenkin et al. studied the synthesis of DME over HNT-supported indium-based formulation [20] and a copper-doped version of the same catalyst [21].

In this study, the performance of an In_2O_3/ZrO_2 catalyst was studied and compared to a commercial CZA catalyst. The synthesis of DME for both catalysts was evaluated in presence of the more conventional HZSM-5 zeolite and with a LTA zeolite, 4A, to also observe the effect of the dehydration catalyst. Finally, some doped formulations were studied, to enhance the reaction performances through the addition of a small quantity of different active sites.

2. Materials and methods

2.1. Catalysts preparation

For this study, methanol synthesis and methanol dehydration catalysts were employed in a physical mixture for the synthesis of DME. For clarity, methanol synthesis catalysts will be generically addressed as MC and methanol dehydration catalysts will be addressed as DC.

As MC, a commercial formulation and several indium-based catalysts were employed. The CZA catalyst (40 wt% CuO, 40 wt% ZnO, 20 wt% Al_2O_3 [22]) employed in this study as benchmark formulation was a commercial sample, provided by BASF under the code K3–110. The HZSM-5 and 4A zeolites employed as dehydration catalysts are also commercial products, respectively provided by Zeolyst and Thermofisher.

The In_2O_3/ZrO_2 based catalysts (labeled as InZr) were synthesized in the laboratory as follows.

InZr catalyst was prepared *via* wet impregnation. A solution in

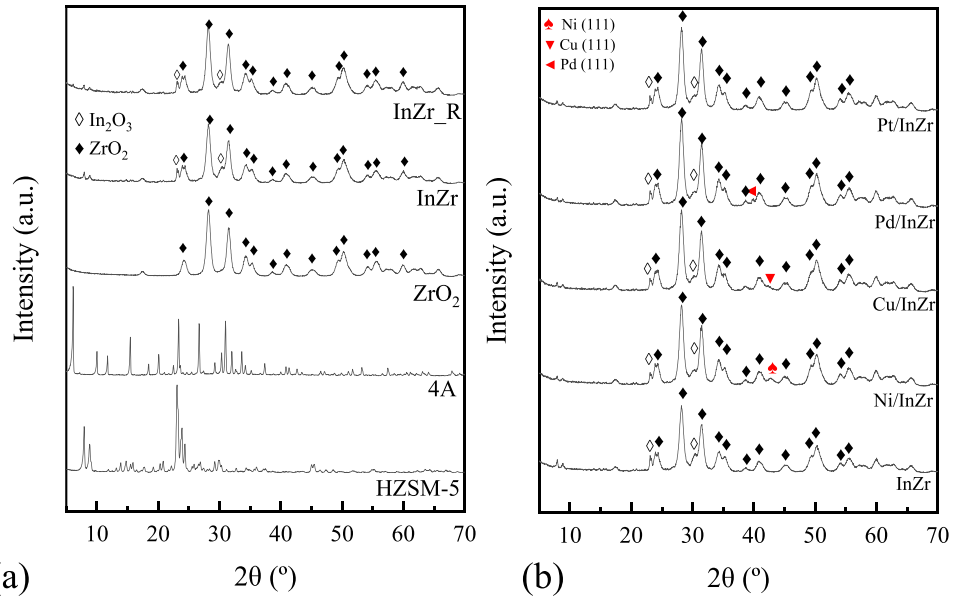

Fig. 2. XRD spectra for the employed catalysts: (a) DC catalysts and ZrO_2, InZr and InZr_R for sake of comparison; (b) Me/InZr samples in their activated (reduced) state. Ni, Cu and Pd are indicated with red symbols.

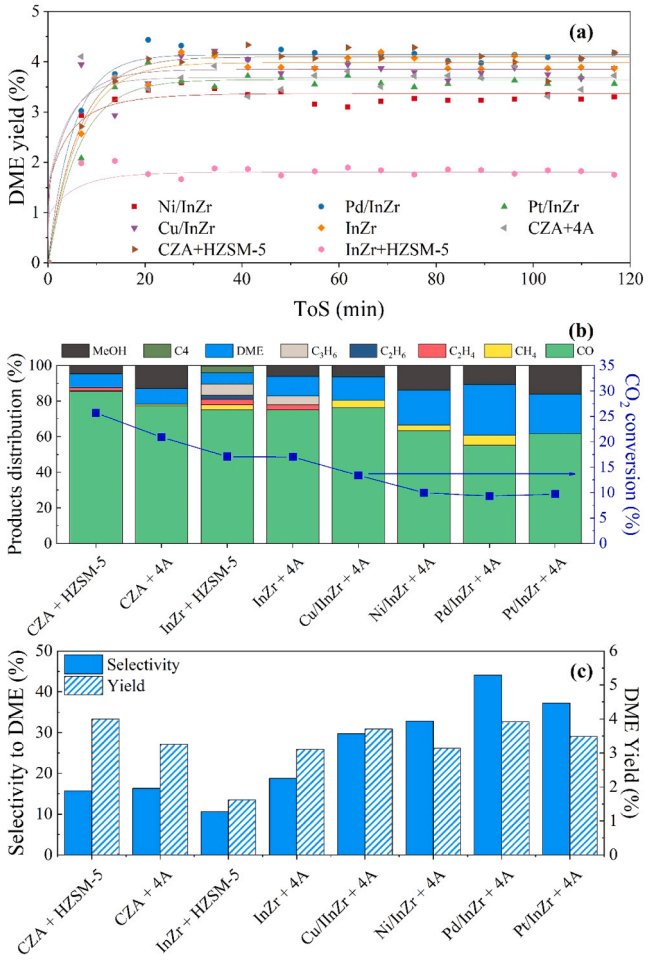

Fig. 3. Preliminary screening of the proposed formulations: effect of the dehydration catalyst and metal doping. Operating conditions: 280 °C, 20 bar and GHSV = 2000 mL(g•h)$^{-1}$ STP. *a) DME yield as a function of time-on-stream (lines for visual guidance only). b) CO_2 conversion and product distribution for each formulation at steady state. c) corresponding yield and selectivity to DME.*

distilled water of indium nitrate ($In(NO_3)_3 \cdot xH_2O$ provided by Sigma Aldrich) was prepared, with the amount of precursor salt corresponding to 9 wt% of metallic indium in the final formulation. The ZrO_2 support (provided by Thermofisher) was added to the solution, and kept stirring at 100 °C to evaporate the whole solvent. The obtained powder was dried overnight at 120 °C and calcined at 500 °C for 3 h, with a heating rate of 2 °C•min^{-1}.

Four Me/InZr catalysts (where Me is either Ni, Cu, Pt or Pd) were prepared to evaluate the addition of a second metal to the formulation. Ni and Cu, which are non-noble metals, were deposited onto the catalyst with the amount of 3 wt%. For both Pt and Pd a loading of 0.5 wt% was set. The bimetallic samples were prepared *via* wet impregnation as well, by depositing the chosen metal on the InZr sample, previously prepared and calcined as above-described. The procedure follows the same step of the InZr. The precursors salt employed for the metals deposition were $Ni(NO_3)_2 \cdot 6\ H_2O$, $Cu(NO_3)_2 \cdot 3\ H_2O$, $PtCl_4$ and $PdCl_2$, all provided by Sigma Aldrich. All the catalysts were dried overnight at 120 °C and calcined at 500 °C for 3 h, with a heating rate of 2 °C•min^{-1}.

All the catalysts were employed with a final dimension of 160–250 μm.

For what concerns the dehydration catalyst, a particle size range of 75–150 μm was fixed. 4A zeolite was bought as 0.4–0.8 mm spheres; hence, it was grinded and sieved to the desired range. HZSM-5 zeolite, on the other hand, was bought as ammonium ZSM-5 from the provider. Hence, it was previously calcined according to [23] to reach the protonic form HZSM-5. Then, because it was a fine powder, to reach the desired dimension it was agglomerated using a binder (Ludox, provided by Sigma Aldrich). The binder is a colloidal silica suspension at 20 wt%, hence the Si:Al ratio of the zeolite resulted slightly modified in the final catalyst, as reported in Table 1. During agglomeration, Ludox coating reduces microporosity and surface area while creating mesopores, likely from interparticle spaces or restructured silica formed during drying (Table 1).

2.2. Experimental setup and procedures

The experimental setup employed for the catalytic tests was composed by three mass flow controllers, a fixed-bed reactor, a condenser for the liquid fraction, a back-pressure controller and the analyzer. The mass flow controllers, as well as the pressure controller,

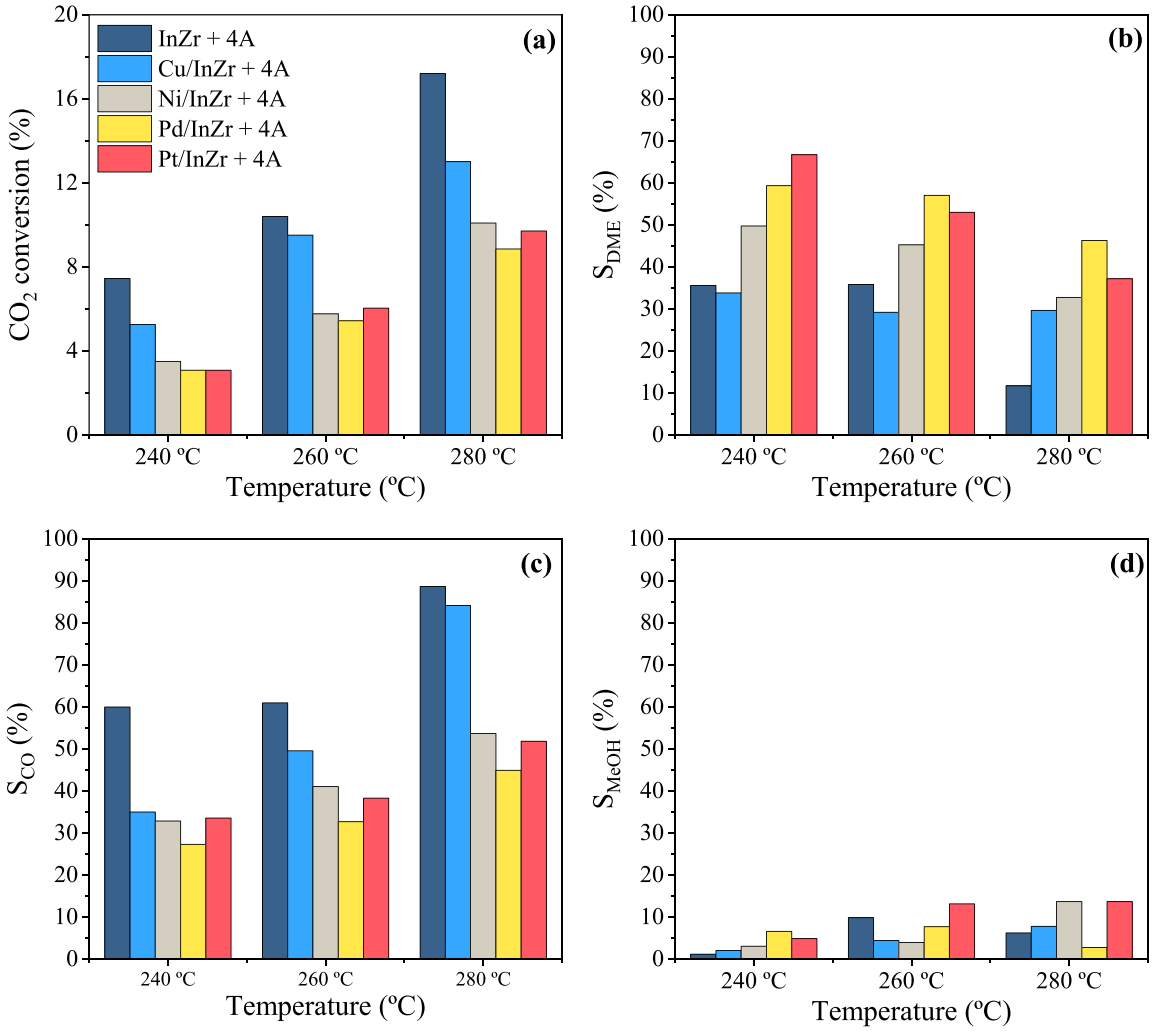

Fig. 4. Doped catalysts performances as a function of temperature. (a) CO_2 conversion; selectivity toward: (b) DME, (c) CO and (d) methanol.

were provided by Brooks. The catalyst was loaded into a 3/4" stainless steel reactor, vertically located in an electrical oven, where the temperature control was realized by means of a K-type thermocouple directly inserted into the catalytic bed. The reactor was equipped with a stainless-steel jacket to ensure a more uniform heat distribution, thus flatter axial and radial temperature profiles. The products stream was cooled at −18 °C to separate the condensable species, which cannot reach the analyzer nor the pressure controller. The dry-base flowrate that leaves the system was measured downstream the pressure controller. The permanent gases were analyzed with a 490 μGC (Agilent) equipped with two columns (HayeSep A and PoraplotQ) and a TCD detector. The condensed liquid was analyzed with a GC-MS QP2010 (Shimadzu) equipped with a TRB-50.2 PONA column (Teknokroma) and a quadrupole mass spectrometer.

For the experiments, a 1:1 wt ratio of the two catalysts was employed, using a total mass of 3 g. The reactants flowrate was fixed at 100 mL•min^{-1} STP, with a stoichiometric ratio of hydrogen and carbon dioxide. No inert was fed into the system, to avoid kinetic limitations due to a lower partial pressure of the reactants. The experiments were conducted with a constant pressure of 20 bar, while the temperature was varied using three values: 240, 260 and 280 °C. Prior to each experiment, the catalyst was activated with a reducing stream (50% H_2 in N_2) at 300 °C for 1 h, with a heating rate of 10 °C/min. Then, the experiment start up was conducted as follows: the system was cooled down to the experiment temperature at natural cooling rate; the reducing stream was changed to the reactants; the system pressure was increased at 1 bar/min to reach the final value of 20 bar. CO_2 conversion X_{CO2}, selectivity and yield to products (S_P and Y_P) were calculated as in Eqs. 10–12, while the products distribution ($X\%_P$) is calculated on the carbonaceous products, according to Eq. 13. In the equations, n represents the molar flows of the i species, the subscript P indicates a generic product and ν is the stoichiometric coefficient of the complete reaction from CO_2 to each product. For the products observed in the present study, these are: 2 for DME (Eq. 1), 1 for methanol (Eq. 2), CO (Eq. 4), and methane (Eq. 5), 2 for ethene (Eq. 6) and ethane (Eq. 7), and 3 for propene (Eq. 8).

$$X_{CO_2} = 1 - \frac{n^{out}_{CO_2}}{n^{in}_{CO_2}} \tag{10}$$

$$Y_P = \frac{n^{out}_P}{\nu_P \bullet n^{in}_{CO_2}} \tag{11}$$

$$S_P = \frac{n^{out}_P}{\nu_P \bullet (n^{in}_{CO_2} - n^{out}_{CO_2})} \tag{12}$$

$$X\%_P = \frac{n^{out}_P}{\sum_P n^{out}_P} \tag{13}$$

2.3. Catalysts characterization

X-ray fluorescence (XRF) to determine the actual composition of the synthesized catalysts was performed in an ARL™ PERFORM'X

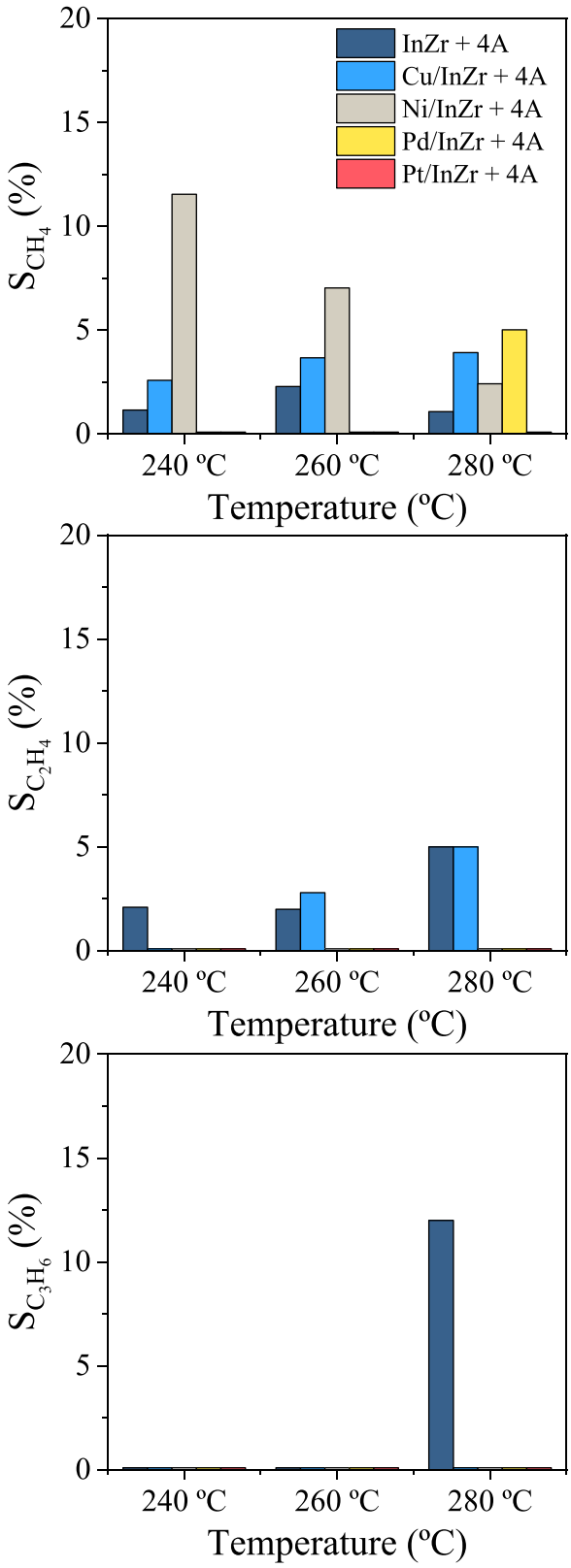

Fig. 5. Selectivity toward minor products: (a) methane; (b) ethylene; (c) propylene.

Sequential X-Ray Fluorescence Spectrometer (ThermoFisher scientific), using the UNIQUANT software for the semiquantitative elemental and oxides analysis.

The crystalline structure of the samples was evaluated *via* X-ray diffractometry (XRD), which was performed in a rotating anode X-ray diffractometer (Rigaku, model Ru2500) with a Cu anode radiation source (40 kV and 80 mA) equipped with a graphite monochromator for the selection of Kα radiation. The analysis condition for XRD are: 2θ in the range 10°–70°, step = 0.03°, t = 1 s/step. The determination of the crystalline phases was performed with the aid of the database JCPDS-International Centre for Diffraction Data-2000.

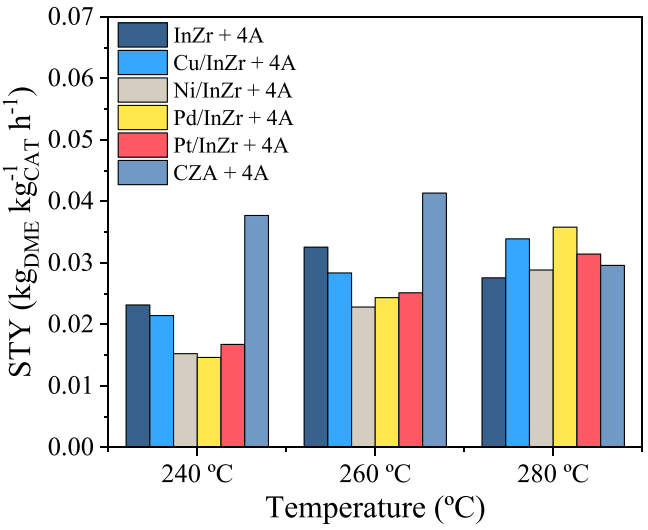

Fig. 6. Comparison between this study's catalysts with the commercial formulation in terms of dimethyl ether STY.

The specific surface area (SSA) and the porous distribution of the samples were evaluated through nitrogen adsorption/desorption at 77 K in a Quantachrome Autosorb iQ3 setup. Prior to analysis, the samples were degassed at 120 °C for 8 h.

The reducibility properties of the sample were evaluated by means of temperature programmed reduction (H_2-TPR), which was performed in an 8 mm diameter quartz reactor: 300 mg of catalyst was loaded into the reactor, and a reducing stream (300 mL•min^{-1} STP, 10% H_2 in N_2) was fed to the system; the temperature was risen with a heating rate of 10 °C•min^{-1} up to 500 °C. The hydrogen consumption was measured through a quadrupole mass spectrometer (ThermoOnix ProLab, by Thermofisher Scientific).

3. Results and discussion

3.1. Catalysts characterization

N_2 adsorption/desorption isotherms were obtained for all the catalysts. The values of specific surface area (SSA), total micropores and mesopores volume – which can be retrieved from this analysis – are reported in Table 1. DC exhibited a type I adsorption isotherm, ascribable to microporous materials such as zeolites. These samples showed a significant amount of micropores, as reported in Table 1, which governs half to almost the total fraction of adsorbed volume. Methanol synthesis catalysts were supported onto ZrO_2, hence all of them have properties similar to the pristine support. All MC isotherms can be classified as type IV isotherms, in which a significant hysteresis is produced due to mesopores presence. It can also be observed that indium addition improves the adsorbed volume of the sample compared to ZrO_2 – leading to the obtainment of a higher SSA value – but subsequently impregnated catalysts Me/In_2O_3/ZrO_2 lost available surface. This phenomenon was more evident in the case of Cu and Ni based catalysts, which have a higher metal loading, while Pt and Pd based ones reported a higher SSA and higher pore volume.

TPR profiles for all samples are reported in Fig. 1. As can be considered comparing the profiles obtained for the Me/InZr

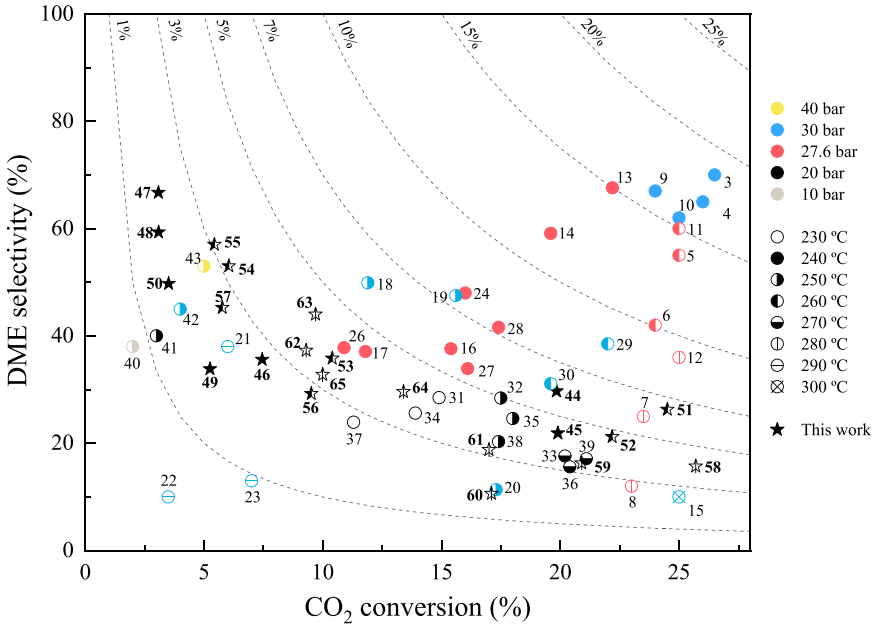

Fig. 7. Outcomes of this study compared to literature results. Legend interpretation: colors are for an immediate visualization of the pressure influence, while different symbols individuate the temperature; a combination of symbol and color gives the operating T and P conditions. The number associate to each figure refers to the reference and additional details in Table 2.

formulations to the InZr alone, all the doping metal oxides can be fully reduced below 300 °C. NiO reduction occurred in two steps, which can be related to its interaction with support: bulk NiO reduces at 200 °C while support-interacting NiO reduces around 300 °C [24,25]. It should be noted that, although the final H_2-TPR temperature reaches 500 °C, the activation procedure prior to activity tests (300 °C under H_2 for 1 h) is sufficient to fully reduce Ni^{2+} to Ni^0, as it will also be supported by XRD analysis of the activated samples, reported in the next section, which indicates the presence of metallic Ni only. Reduction peaks above 500 °C, typically associated with spinel-like structures, are unlikely under the current experimental conditions. Copper oxide presented a single reduction peak below 200 °C, according to literature [26]. Pt oxide reduction occurred with a sharp peak around 150 °C [27,28], while Pd oxide was reduced along a broader temperature range, around 200 °C [29]. The reduction of doping metal oxides can be observed alongside In_2O_3 reduction, which also occurred in the InZr sample. This result agrees well with the current literature; in addition, In_2O_3 is reported to complete its reduction up to 700 °C [18,30]. The observed behavior means that In_2O_3 reduction is not produced by the presence of another species, even though the existence of other metals can induce a change in the reducibility properties of indium oxide. It can be noticed, indeed, that In_2O_3 reduction occurred consequently NiO and CuO reduction – and the reduction profile is characterized by unified peaks – while it had a different behavior in presence of noble metals. The Pd/InZr formulation displayed a marked peak at low temperature that can be ascribed to the reduction of Pd and In oxides at the same time. This marked anticipation of In_2O_3 reduction was already reported by Pinheiro Araújo et al. [31], who observed indium oxide shifting from 191 to 107 °C. As well, the peak at higher temperature, around 400 °C, can be attributed to the shift to lower temperature of less reducible In_2O_3 [32]. On the other hand, the Pt/InZr formulation displayed two completely different reduction peaks for Pt oxide and In oxide. The peaks at 150 °C and 350–450 °C are, however, in good agreement with the work of Sun et al. [33] and Liu et al. [34], who observed In_2O_3 reduction around 400 °C. Since spillover is a phenomenon which occurrence is typical in presence of noble metals, it appears unusual to observe spillover for the Pd/InZr sample and not for the Pt/InZr sample. This suggested that Pd and Pt interact differently with the support, with indium having a much stronger interaction with palladium rather than platinum.

XRD spectra for the fresh catalysts are displayed in Fig. 2. Since DC were not functionalized with additional species, their spectra (Fig. 2a) showed the diffraction peaks characteristic of ZSM-5 (JCPDS card No. 44–0003) and 4A (JCPDS card No. 39–222) structures. It is worth noting that no modification in the crystalline structure of agglomerated HZSM-5 zeolite was observed while comparing the sample to the standard. The ZrO_2 spectrum showed all the peaks characteristic of the monoclinic form. Because of the complexity of this spectrum, also the individuation of other species resulted complicated. Indium oxide existence in the sample InZr can be only appreciated with a peak at 22.5° and 30.4° corresponding to In_2O_3 (112) and In_2O_3 (222) respectively [35], the latter visible as a shoulder of the zirconia peak at 31.44°. Me/InZr formulations are obtained as Me_xO_y after calcination, therefore they need to be activated in hydrogen to obtain the metallic form of Ni, Cu, Pd, and Pt which are the active species. During activation, In_2O_3 is also reduced as observed from the TPR. For this reason, activated InZr, labeled as InZr_R, was also analyzed. As can be observed from Fig. 2a, XRD spectrum for InZr_R preserves the peaks of the calcined sample, even though a reduction in the peaks of In_2O_3 (222) is visible, indicating that – as hypothesized – In_2O_3 reduction is only partial during activation and the majority of the indium maintains its fully oxidized state. XRD spectra for the samples Me/InZr (Fig. 2b) were obtained for activated samples, to observe the catalysts samples as they are employed in the reaction. Besides metallic species should display several peaks, it is only possible to distinguish Ni (111), Cu (111) and Pd (111) peaks [36–38] – highlighted in red in Fig. 2 – while Pt was not observable in the obtained spectrum. In all samples, peaks related to In_2O_3 are clearly visible.

3.2. Preliminary screening

A preliminary assessment of the catalytic performance was conducted under fixed temperature conditions, with a set temperature of 280 °C. This temperature was chosen as it facilitated high conversion rates without a significant loss in selectivity toward the desired product. The results of this study are presented in Fig. 3. For this preliminary screening, each catalyst was tested for a maximum time of 2 h at a single

Table 2
Comparison with literature. Progressive numbering of the literature results allows a better interpretation of Fig. 7.

Ref.	No.	MC type	DC	DC:MC	P (MPa)	T(°C)	Catalyst specification from Ref.
[51]	1	CZAWI	Al_2O_3	74 % Al_2O_3	2.5	230	Al_2O_3 as support
	2	CZACP	-		2.5	230	
[52]	3	CZZA	HZSM−5	1:1	2.76	240	CZZA 4/2/1/0.5
	4					240	CZZA 4/2/1.5/0.5
	5					260	CZZA 4/2/1/0.5
	6					260	CZZA 4/2/1.5/0.5
	7					280	CZZA 4/2/1/0.5
	8					280	CZZA 4/2/1.5/0.5
[53]	9	CZA	HZSM−5	1:1	2.76	240	
	10			10:1		240	
	11			1:1		260	
	12			1:1		280	
[54]	13	CZZ	HZSM−5	10:1	3	240	CZZH300
	14						CZZH600
[16]	15	CZZ	SAPO−11	1:2	3	300	
[55]	16	CZZ	HZSM−5	1:2	3	240	
	17						
[56]	18	CuO–TiO_2–ZrO_2	HZSM−5	2:1	3	250	CuO–TiO_2–ZrO_2 0/100
	19						CuO–TiO_2–ZrO_2 50/50
	20						CuO–TiO_2–ZrO_2 100/0
[57]	21	Pd/In_2O_3	HZSM−5	1:2	3	290	MM
	22						DB
	23						GM
[58]	24	CZZ	HZSM−5	1:1	3	240	ZZ-M
	25				1	220	ZZ-M
[59]	26	CZZ	HZSM−5	2:1	3	240	ZZ-G grinded
	27						ZZ-M mixed
[60]	28	CZZ	FER8	1:1	3	240	
	29					260	
	30					260	Mech. mixing
[61]	31	CZZ	FER	2:1	2	230	CZZ(C) coprec
	32					250	CZZ(C)
	33					270	CZZ(C)
	34					230	CZZ(G) sol gel
	35					250	CZZ(G)
	36					270	CZZ(G)
	37					230	CZZ(S) grinding
	38					250	CZZ(S)
	39					270	CZZ(S)
[20]	40	In_2O_3/Al-MCM−41/HNT	-	-	1	250	
	41				2		
	42				3		
	43				4		
	44–65	This work					

temperature, during which no deactivation was observed, to avoid measuring a misleading value of activity. The DME yield as a function of the time-on-stream (ToS) is reported in Fig. 3(a). It can be observed that, after an initial transient time, the system reached the steady state: all the investigated catalytic systems (MC + DC) demonstrated to be stable during the experiment time.

To better discuss the catalytic performances, the products distribution and the DME yield and selectivity were given respectively in Fig. 3 (b) and (c). The novel InZr catalyst, in combination with the conventional DME synthesis zeolite HZSM-5, yielded deceiving results when compared to the benchmark formulation. As reported by Martin et al. [39] this catalyst was supposed to be not only more stable yet more active in methanol synthesis than conventional CZA catalysts. Instead, as depicted in Fig. 3(b) the DME production was lower than awaited, and a broad spectrum of other products - in addition to CO (which was expected) - was observed, including methane, ethane, ethylene, propylene, and butene. A negligible amount of methanol was recovered in the liquid phase during the experiment (nearly imperceptible in the graph). On the other hand, the CZA catalyst exhibited significantly higher CO_2 conversion and a narrower product distribution, where the only detected carbonaceous products were methanol, DME, C_2H_4, and CO. At first glance, the CZA+HZSM-5 system appears to offer superior performance, primarily due to its higher DME production and fewer side reactions. However, when considering additional factors, this advantage is not necessarily reflected in overall performance. It is important to note that despite the fewer by-products, the CZA+HZSM-5 system promoted the reverse water-gas shift (rWGS) reaction to a greater extent compared to the InZr+HZSM-5 system. In addition, CZA is widely reported to be deactivated in the presence of water [40,41].

The replacement of the dehydration catalyst led to a marked alteration in the overall process performance. Substituting HZSM-5 with 4A zeolite led to a decline in CO_2 conversion for both catalytic systems. This decrease in conversion was more pronounced in the InZr system compared to the CZA system, and in both instances, it was accompanied by an increase in the methanol yield. These findings indicate that the 4A zeolite exhibits a lower dehydration capacity than HZSM-5. To a certain extent, this result can be attributed to the different acidity of the two zeolites; in particular, the protonic HZSM-5 zeolite is rich of Brønsted acid sites, which are the most effective in methanol dehydration [42]. Indeed, the target product, dimethyl ether, is formed via the acid-catalyzed dehydration of methanol, thus the acidity of the DC catalyst is a major concern. However, shape selectivity and diffusion limitations are also critical factors. The structural characteristics of zeolite 4A (LTA framework) – particularly its small 8-membered ring (8-MR) pore openings (~4.1 Å) – play a significant role in its catalytic behavior. These narrow pores limit the accessibility of internal acid sites and restrict the diffusion of methanol and reaction intermediates, which can reduce the overall dehydration activity compared to medium-pore

zeolites like HZSM-5 (MFI framework) [43]. Moreover, the LTA structure lacks the larger cavities and channel intersections found in MFI-type zeolites, which are known to stabilize transition states and facilitate the formation of reaction intermediates. This structural constraint likely contributes to the lower DME productivity observed with 4A, as the dehydration reaction requires not only accessible acid sites but also sufficient space for methanol dimerization and water desorption [44,45]. Furthermore, LTA frameworks are often used in membrane applications to selectively adsorb water over methanol [46]: this could indicate that there could be preferential adsorption of water rather than methanol, which may also influence the catalytic performance by favoring water retention and hindering methanol access to active sites.

All these factors could have had an impact also on the dehydration selectivity of zeolite 4A, compared to HZSM-5. Specifically, the product distribution was narrower in the presence of 4A zeolite, with a strongly reduced or nearly absent production of hydrocarbons (C_xH_y). A comparison of selectivity and yield from Fig. 3(c) reveals two key observations. For both InZr and CZA, the change from HZSM-5 to 4A slightly enhanced DME selectivity; however, because of the differences in CO_2 conversion, this led to a noteworthy increase in DME yield for the InZr system, and a decrease for the CZA system. It is important to consider that the more pronounced hydrocarbons production over the InZr+HZSM-5 system was detrimental for the yield to DME; therefore, their elimination through the employment of 4A zeolite resulted highly beneficial. Overall, it is possible to state that the utilization of 4A as dehydration catalyst surely hinders the total reaction; however, due to its extreme selectivity, the employment of this zeolite can be beneficial in systems in which the methanol catalyst is more selective, to reduce the overall production of other gaseous compounds.

The modification of the InZr catalyst with different metals was also evaluated at screening conditions and in presence of the 4A zeolite, and it is reported in Fig. 3. The first thing that can be observed is that there is not a well-defined trend between the employment of transition metals and noble metals. Furthermore, the addition of a second metal seemed to worsen the activity of the indium-based catalyst. A CO_2 conversion of 13 % was observed for the Cu/InZr catalyst, which was the highest among the promoted catalysts, but it was lower than the unpromoted InZr formulation (Fig. 3b). However, relevant changes in selectivity occurred in presence of the promoted samples. The addition of a second metal allowed to hinder the production of higher hydrocarbons, while the promotion with platinum eliminated all the hydrocarbon byproducts, including methane. In terms of selectivity and yield to DME (Fig. 3c), the highest values were found in presence of the noble metals, and in particular with the Pd-promoted catalyst. However, it is worth noting that the Ni-based and Cu-based formulation also improved the selectivity toward DME, giving a total yield to the product comparable to the unpromoted catalyst despite their lower reactants conversion.

3.3. Activity tests

A deeper analysis of the behavior of the doped formulation was conducted by performing tests at lower temperature, at which methanol and DME production are thermodynamically favored. The results in terms of CO_2 conversion and selectivity toward the most relevant products are resumed in Fig. 4. As can be observed, the doping of the InZr catalysts with any of the chosen metals drove the selectivity of the process toward DME formation also at lower temperatures, enhancing the effect already ensured by the thermodynamic equilibrium of the process.

Also, as observed at 280 °C, modifying the InZr formulation with the addition of other active metals changed the selectivity toward undesired products such methane and small olefins. As reported in Fig. 5, small olefins formation was promoted at higher temperatures, and the addition of either Ni, Pt or Pd to the formulation completely avoid their formation in the whole temperature range. On the other hand, methane synthesis was promoted by low temperature, and it is enhanced by the addition of other metals, especially Ni, which is widely recognized to be a so-called methanizer species [47,48]. The only exception was observed for Pt/InZr formulation, which totally suppressed methane formation at any temperature. The suppression of methane formation over Pt/InZr likely involves a combination of factors beyond the intrinsic catalytic activity of Pt, including effect of adsorption strength and support acidity. Since in this study the InZr support is common to all the metallic formulations, differences in acidity are unlikely to explain the observed suppression of methane on Pt/InZr. Regarding the other aspects, it is important to observe that while Pt is a noble metal with excellent hydrogen activation properties, it is also well known to strongly adsorb CO, often leading to CO poisoning in catalytic systems. This strong CO binding can inhibit further hydrogenation steps required for methane formation, particularly in the absence of co-catalysts or promoters.

Based on a previous experimental work, we have observed that Pt alone does not catalyze methanation effectively unless another active species is present [49]. This supports the interpretation that the lack of methane formation is not due to a lack of hydrogen activation or CO activation (Pt has an outstanding capacity of reducing CO_2 to CO [50]), but rather to inhibited CO hydrogenation, likely due to strong CO adsorption and the absence of suitable sites for further transformation [49,50].

Finally, a comparison can be made between the studied catalysts and the commercial formulation selected as benchmark for this work. The most valuable result to be considered for a scaled-up application surely is represented by the space time yield (STY) of produced DME, calculated as kg of DME synthesized per gram of catalyst and unit of time (generally hours). The outcomes are displayed in Fig. 6. As can be observed, at high temperature, where the catalysts demonstrated to be more active, the STY obtained with any of the catalysts in this study is comparable, if not higher, than the one reached by the commercial formulation. When the temperature was decreased, the STY achieved with the proposed formulations was always lower than the CZA+ 4A system, reflecting the lower activity of the InZr-based catalysts. Activity alone, however, is not sufficient for process optimisation; selectivity must also be considered. Although CZA + 4A maintained a higher STY at lower temperatures, it exhibited markedly poorer selectivity toward DME, which would lead to the accumulation of undesired by-products in any recycle loop. To enhance the single-pass conversion, in fact, recirculating a fraction of the products stream is often a valuable option. Increased concentrations of undesired species can accelerate coke formation through secondary reactions (e.g., polymerization of light olefins), further decreasing overall DME selectivity. Consequently, despite their lower low-temperature STY, the InZr-based catalysts may afford a more favourable overall process performance once reactor temperature and recycle ratio are optimised.

Overall, the results obtained in this study are well aligned with current literature. A visual comparison is given in Fig. 7, in which the data are collected in a DME selectivity vs CO_2 conversion graph. All results have been progressively numbered (Table 2) to distinguish any other parameter which was not disclosed in the figure, such as the type of MC and DC catalysts, and the ratio MC:DC employed. Iso-yield *loci* can be represented in this graph as hyperbolic functions (dotted lines), which can guide the reader in the interpretation. As can be easily observed from the colour pattern, high DME yields can be obtained almost exclusively at high pressure: all the literature values that exceed a DME yield of 7 % were obtained at pressure of 27.6 bar or higher. In the present study, represented by star markers, the DME yield ranges from 1 % to 5 %. Comparable yields have also been reported in numerous literature studies conducted at equal or higher pressures within the temperature range of 230–300 °C. Considered the promoting effect of the operating pressure, it is noticeable that – with the catalysts proposed in this study – it was possible to reach roughly the same yield, or even overcome some literature results, obtained at higher pressures. This result further adds value to the MC formulations prepared, when considering that the 4A zeolite employed in this study was observed to

have a lower dehydration capacity compared to the more conventional HZSM-5.

4. Conclusions

In this work, single-pass DME synthesis was carried out using novel catalytic formulations. Built on the established enhanced stability of indium-doped formulations for methanol synthesis, this study focused on synthesizing indium-modified catalysts using monoclinic zirconia as the support and incorporating Ni, Cu, Pt, and Pd as active metal components for the production of dimethyl ether. The substitution of the most conventional HZSM-5 zeolite as dehydration catalyst with 4A zeolite was also evaluated. As outcome, it was observed that 4A zeolite has a lower dehydration ability, although this determined an overall increase in the selectivity of the process. In addition, it was noticed that the addition of further compounds to an InZr formulation decreased its activity, but it enhanced the selectivity toward the desired product resulting in an overall increased yield to DME. The activity of Me/InZr catalysts was found to decrease while diminishing the operating temperature. The production of byproducts such as light olefins and methane was found to be strongly dependent on the metal employed in the formulation: Ni, Pt and Pd allowed to decrease the production of light olefins, although Ni strongly incremented methane production. Only Pt/InZr formulation allowed to hinder completely the production of byproducts in the whole temperature range. Compared to a conventional CZA catalyst coupled with 4A zeolite, the studied catalysts achieved in general lower DME space time yields (STY), reaching a comparable value only at 280 °C. Nevertheless, the improved selectivity of these formulations made them particularly suitable in the perspective of operating with a recycle loop.

CRediT authorship contribution statement

Javier Herguido: Writing – review & editing, Validation, Supervision, Resources, Funding acquisition. **Simona Renda:** Writing – original draft, Visualization, Validation, Software, Methodology, Investigation, Funding acquisition, Formal analysis, Data curation, Conceptualization. **Jaime Soler:** Writing – review & editing, Validation, Supervision, Resources, Funding acquisition. **Miguel Menéndez:** Writing – review & editing, Validation, Supervision, Resources, Project administration, Funding acquisition, Conceptualization.

Funding

This research is part of the CIMZATE project (grant no. PLEC2022-009239) funded by MCIN/AEI/10.13039/501100011033 and NextGenerationEU/PRTR. S.R. acknowledges the funding of the Juan de la Cierva fellowship (grant no. JDC2023-052947-I) by MCIU/AEI/10.13039/501100011033 and FSE+. The consolidated research group Catalysis and Reactor Engineering Group (CREG, T43–23R) has the financial support of Gobierno de Aragón through the European Social Fund – FEDER. All authors acknowledge the use of *Servicio general de Apoyo a la Investigación* – SAI (University of Zaragoza) for the characterization of the samples.

Declaration of Competing Interest

The authors declare that they have no known competing financial interests or personal relationships that could have appeared to influence the work reported in this paper.

Data Availability

Data will be made available on request.

References

[1] V. Dieterich, A. Buttler, A. Hanel, H. Spliethoff, S. Fendt, Energy Environ. Sci. 13 (2020) 3207–3252, https://doi.org/10.1039/d0ee01187h.
[2] Z. Azizi, M. Rezaeimanesh, T. Tohidian, M.R. Rahimpour, Chem. Eng. Process. Process. Intensif. 82 (2014) 150–172, https://doi.org/10.1016/J.CEP.2014.06.007.
[3] A. Lotfollahzade Moghaddam, M. Ghavipour, J. Kopyscinski, M.J. Hazlett, Appl. Catal. A Gen. 672 (2024) 119594, https://doi.org/10.1016/J.APCATA.2024.119594.
[4] C. Arcoumanis, C. Bae, R. Crookes, E. Kinoshita, Fuel 87 (2008) 1014–1030, https://doi.org/10.1016/J.FUEL.2007.06.007.
[5] S.H. Park, C.S. Lee, Energy Convers. Manag 86 (2014) 848–863, https://doi.org/10.1016/J.ENCONMAN.2014.06.051.
[6] T.T.N. Vu, A. Desgagnés, M.C. Iliuta, Appl. Catal. A Gen. 617 (2021), https://doi.org/10.1016/j.apcata.2021.118119.
[7] M. Gentzen, D.E. Doronkin, T.L. Sheppard, J.D. Grunwaldt, J. Sauer, S. Behrens, Appl. Catal. A Gen. 562 (2018) 206–214, https://doi.org/10.1016/J.APCATA.2018.04.018.
[8] A. Ateka, P. Rodriguez-Vega, J. Ereña, A.T. Aguayo, J. Bilbao, Fuel Process. Technol. 233 (2022), https://doi.org/10.1016/j.fuproc.2022.107310.
[9] S. Renda, J. Soler, J. Herguido, M. Menéndez, Biomass. Bioenergy 197 (2025), https://doi.org/10.1016/j.biombioe.2025.107764.
[10] G. Jia, Y. Tan, Y. Han, Ind. Eng. Chem. Res. 45 (2006) 1152–1159, https://doi.org/10.1021/ie050499b.
[11] S. Renda, M. Menéndez, Catalysts 15 (2025) 509, https://doi.org/10.3390/catal15060509.
[12] Y. Wei, J. Liu, H. Li, X. Zhang, Y. Zhang, J. Yang, M. Wang, Z. Liu, Z. Yan, Appl. Catal. A Gen. 700 (2025) 120286, https://doi.org/10.1016/J.APCATA.2025.120286.
[13] H.Y. Chen, J. Pihl, T.J. Toops, S. Sinha Majumdar, Appl. Catal. A Gen. 656 (2023) 119140, https://doi.org/10.1016/J.APCATA.2023.119140.
[14] R. Montesano, A. Narvaez, D. Chadwick, Appl. Catal. A Gen. 482 (2014) 69–77, https://doi.org/10.1016/J.APCATA.2014.05.009.
[15] A. Prašnikar, A. Pavlišič, F. Ruiz-Zepeda, J. Kovač, B. Likozar, Ind. Eng. Chem. Res. 58 (2019) 13021–13029, https://doi.org/10.1021/acs.iecr.9b01898.
[16] A. Ateka, A. Portillo, M. Sánchez-Contador, J. Bilbao, A.T. Aguayo, Renew. Energy 169 (2021) 1242–1251, https://doi.org/10.1016/j.renene.2021.01.062.
[17] Y. Zhang, H. Ding, L. Li, K. Zhu, J. Liu, Appl. Catal. A Gen. 632 (2022) 118483, https://doi.org/10.1016/J.APCATA.2022.118483.
[18] J. Su, D. Wang, Y. Wang, H. Zhou, C. Liu, S. Liu, C. Wang, W. Yang, Z. Xie, M. He, ChemCatChem 10 (2018) 1536–1541, https://doi.org/10.1002/cctc.201702054.
[19] A. Porta, C. Coffano, M. Piacentini, F. Rabino, B. Picutti, L. Lietti, C.G. Visconti, Appl. Catal. A Gen. 682 (2024) 119799, https://doi.org/10.1016/J.APCATA.2024.119799.
[20] A. Pechenkin, D. Potemkin, S. Badmaev, E. Smirnova, K. Cherednichenko, V. Vinokurov, A. Glotov, Green. Process. Synth. 10 (2021) 594–605, https://doi.org/10.1515/gps-2021-0058.
[21] A. Pechenkin, D. Potemkin, M. Rubtsova, P. Snytnikov, P. Plyusnin, A. Glotov, Catalysts 11 (2021), https://doi.org/10.3390/catal11101151.
[22] T.A. Semelsberger, K.C. Ott, R.L. Borup, H.L. Greene, Appl. Catal. B 61 (2005) 281–287, https://doi.org/10.1016/J.APCATB.2005.05.014.
[23] M. Menéndez, R. Ciércoles, J. Lasobras, J. Soler, J. Herguido, Catalysts 14 (2024) 409, https://doi.org/10.3390/catal14070409.
[24] J. Zhu, F. Cannizzaro, L. Liu, H. Zhang, N. Kosinov, I.A.W. Filot, J. Rabeah, A. Brückner, E.J.M. Hensen, ACS Catal. 11 (2021) 11371–11384, https://doi.org/10.1021/acscatal.1c03170.
[25] Y. Wu, K. Xu, J. Tian, L. Shang, K.B. Tan, H. Sun, K. Sun, X. Rao, G. Zhan, ACS Appl. Mater. Interfaces 16 (2024) 16186–16202, https://doi.org/10.1021/acsami.3c19311.
[26] J.I. Makiura, T. Higo, Y. Kurosawa, K. Murakami, S. Ogo, H. Tsuneki, Y. Hashimoto, Y. Sato, Y. Sekine, Chem. Sci. 12 (2021) 2108–2113, https://doi.org/10.1039/d0sc05340f.
[27] M. Martinelli, R. Garcia, C.D. Watson, D.C. Cronauer, A.J. Kropf, G. Jacobs, Nanomaterials 11 (2021), https://doi.org/10.3390/nano11092233.
[28] T. Shi, Y. Men, S. Liu, J. Wang, Z. Li, K. Qin, D. Tian, W. An, X. Pan, L. Li, Colloids Surf. A Physicochem Eng. Asp. 651 (2022) 129782, https://doi.org/10.1016/J.COLSURFA.2022.129782.
[29] G. Tian, Y. Wu, S. Wu, S. Huang, J. Gao, Catal. Lett. 153 (2023) 903–910, https://doi.org/10.1007/s10562-022-04030-2.
[30] T. Pinheiro Araújo, C. Mondelli, M. Agrachev, T. Zou, P.O. Willi, K.M. Engel, R. N. Grass, W.J. Stark, O.V. Safonova, G. Jeschke, S. Mitchell, J. Pérez-Ramírez, Nat. Commun. 13 (2022), https://doi.org/10.1038/s41467-022-33391-w.
[31] T.P. Araújo, J. Morales-Vidal, G. Giannakakis, C. Mondelli, H. Eliasson, R. Erni, J. A. Stewart, S. Mitchell, N. López, J. Pérez-Ramírez, Angew. Chem. Int. Ed. 62 (2023), https://doi.org/10.1002/anie.202306563.
[32] Z. Li, Y. Men, S. Liu, J. Wang, K. Qin, D. Tian, T. Shi, L. Zhang, W. An, Appl. Surf. Sci. 603 (2022) 154420, https://doi.org/10.1016/J.APSUSC.2022.154420.
[33] K. Sun, C. Shen, R. Zou, C. jun Liu, Appl. Catal. B 320 (2023) 122018, https://doi.org/10.1016/J.APCATB.2022.122018.
[34] X. Liu, Y. Men, J. Wang, R. He, Y. Wang, J. Power Sources 364 (2017) 341–350, https://doi.org/10.1016/J.JPOWSOUR.2017.08.043.
[35] H. Ullah, Z.H. Yamani, A. Qurashi, J. Iqbal, K. Safeen, J. Mater. Sci. Materials Electron. 31 (2020) 17474–17481, https://doi.org/10.1007/s10854-020-04303-9.
[36] H. Wang, X. Kou, J. Zhang, J. Li, Bull. Mater. Sci. 31 (2008) 97–100, https://doi.org/10.1007/s12034-008-0017-1.

[37] A. Nasirian, J. Nano Dim 2 (2012) 159–164.
[38] L. Xu, X.C. Wu, J.J. Zhu, Nanotechnology 19 (2008), https://doi.org/10.1088/0957-4484/19/30/305603.
[39] O. Martin, A.J. Martín, C. Mondelli, S. Mitchell, T.F. Segawa, R. Hauert, C. Drouilly, D. Curulla-Ferré, J. Pérez-Ramírez, Angew. Chem. 128 (2016) 6369–6373, https://doi.org/10.1002/ange.201600943.
[40] A. Prašnikar, A. Pavlišič, F. Ruiz-Zepeda, J. Kovač, B. Likozar, Ind. Eng. Chem. Res. 58 (2019) 13021–13029, https://doi.org/10.1021/acs.iecr.9b01898.
[41] S. Ay, M. Ozdemir, M. Melikoglu, Chem. Eng. Res. Des. 175 (2021) 146–160, https://doi.org/10.1016/J.CHERD.2021.08.039.
[42] A. García-Trenco, A. Martínez, Appl. Catal. A Gen. 411412 (2012) 170–179, https://doi.org/10.1016/J.APCATA.2011.10.036.
[43] S. Wang, Z. Qin, M. Dong, J. Wang, W. Fan, Chem. Catal. 2 (2022) 1657–1685, https://doi.org/10.1016/J.CHECAT.2022.05.012.
[44] J. Xie, U. Olsbye, Chem. Rev. 123 (2023) 11775–11816, https://doi.org/10.1021/acs.chemrev.3c00058.
[45] G. Seo, J.H. Kim, H.G. Jang, Catal. Surv. Asia 17 (2013) 103–118, https://doi.org/10.1007/s10563-013-9157-4.
[46] M. Seshimo, B. Liu, H.R. Lee, K. Yogo, Y. Yamaguchi, N. Shigaki, Y. Mogi, H. Kita, S.-I. Nakao, (2021). doi: 10.3390/membranes.
[47] V.D. Mercader, P. Durán, P. Aragüés-Aldea, E. Francés, J. Herguido, J.A. Peña, Catal. Today 433 (2024), https://doi.org/10.1016/j.cattod.2024.114667.
[48] S. Renda, M. Martino, V. Palma, J. Clean. Prod. 434 (2024), https://doi.org/10.1016/j.jclepro.2023.140221.
[49] S. Renda, A. Ricca, V. Palma, Int. J. Hydrog. Energy 46 (2021), https://doi.org/10.1016/j.ijhydene.2020.05.093.
[50] V. Palma, R. Goodall, A. Thompson, C. Ruocco, S. Renda, R. Leach, M. Martino, Int. J. Hydrog. Energy 46 (2021), https://doi.org/10.1016/j.ijhydene.2020.04.065.
[51] R.G. Santiago, J.A. Coelho, S.M.P. de Lucena, A.P.S. Musse, M. de, F. Portilho, E. Rodriguez-Castellón, D.C.S. de Azevedo, M. Bastos-Neto, Front Chem. 10 (2022), https://doi.org/10.3389/fchem.2022.903053.
[52] S. Ren, X. Fan, Z. Shang, W.R. Shoemaker, L. Ma, T. Wu, S. Li, N.B. Klinghoffer, M. Yu, X. Liang, J. CO2 Util. 36 (2020) 82–95, https://doi.org/10.1016/J.JCOU.2019.11.013.
[53] S. Ren, S. Li, N. Klinghoffer, M. Yu, X. Liang, Carbon Resour. Convers. 2 (2019) 85–94, https://doi.org/10.1016/J.CRCON.2019.03.002.
[54] L. Li, D. Mao, J. Xiao, L. Li, X. Guo, J. Yu, Chem. Eng. Res. Des. 111 (2016) 100–108, https://doi.org/10.1016/J.CHERD.2016.04.018.
[55] F. Frusteri, G. Bonura, C. Cannilla, G. Drago Ferrante, A. Aloise, E. Catizzone, M. Migliori, G. Giordano, Appl. Catal. B 176–177 (2015) 522–531, https://doi.org/10.1016/j.apcatb.2015.04.032.
[56] S. Wang, D. Mao, X. Guo, G. Wu, G. Lu, Catal. Commun. 10 (2009) 1367–1370, https://doi.org/10.1016/J.CATCOM.2009.02.001.
[57] K.B. Tan, P. Tian, X. Zhang, J. Tian, G. Zhan, J. Huang, Q. Li, Sep Purif. Technol. 297 (2022) 121559, https://doi.org/10.1016/J.SEPPUR.2022.121559.
[58] G. Bonura, M. Cordaro, C. Cannilla, A. Mezzapica, L. Spadaro, F. Arena, F. Frusteri, Catal. Today 228 (2014) 51–57, https://doi.org/10.1016/j.cattod.2013.11.017.
[59] G. Bonura, M. Cordaro, L. Spadaro, C. Cannilla, F. Arena, F. Frusteri, Appl. Catal. B 140–141 (2013) 16–24, https://doi.org/10.1016/J.APCATB.2013.03.048.
[60] G. Bonura, M. Migliori, L. Frusteri, C. Cannilla, E. Catizzone, G. Giordano, F. Frusteri, J. CO2 Util. 24 (2018) 398–406, https://doi.org/10.1016/J.JCOU.2018.01.028.
[61] Q. Sheng, R.P. Ye, W. Gong, X. Shi, B. Xu, M. Argyle, H. Adidharma, M. Fan, J. Environ. Sci. 92 (2020) 106–117, https://doi.org/10.1016/J.JES.2020.02.015.